ISSN No: 2348-4845
International Journal & Magazine of Engineering, Technology, Management and Research
A Peer Reviewed Open Access International Journal

Medium Voltage High-Power Converter Topology for 10MW Wind Generation with the Large Permanent Magnet Wind Generator Systems

B. Sri Nandini
M.Tech (Power Systems)
KSRM College of Engineering, Kurnool.

Mr. Bhaskar Reddy
Associate Professor
KSRM College of Engineering, Kurnool.

ABSTRACT

This paper proposes a modular, medium voltage, high-power converter topology for the large permanent magnet wind generator system, eliminating the grid-side step-up transformer, which is desirable for both onshore and offshore wind turbines. The power conversion systems for large wind turbines are facing a great challenge as today's wind turbine power outputs approach 5 MW and above. The conventional low voltage power conversion system will suffer from a high transmission current, which significantly increases losses and cost of the cables as well as voltage drop. The converter modules are cascaded to achieve medium voltage output. Each converter module is fed by a pair of generator coils with 90 phase shift to get the stable dc-link power. At the grid-side, H-bridge inverters are connected in series to generate multilevel medium voltage output and the voltage- oriented vector control scheme is adopted to regulate the converter active and reactive power transferred to the grid. The power factor correcn (PFC) circuit enables the generator to achieve unity power factor operation and the generator armature inductance is used as ac-side PFC boost inductance. Simulation results with a 2-MW wind turbine system and experimental results with a down-scaled 3-kW system validate the proposed topology and control methods. The proposed system can successfully deliver power from the wind generator to the grid.

INTRODUCTION

Today, the most popular large variable-speed wind turbines are rated around 1.5–3 MW. Nevertheless, 7-MW wind turbines have recently appeared and even larger wind turbines, e.g., 10MW, are under development in order to reduce the unit cost of wind power generation [1], [2]. Wind turbines equipped with direct-drive permanent magnet generators (PMGs) and full power converters are generally favored due to simplified drive train structure and thus higher reliability, especially for offshore applications, compared with the doubly fed induction generator-based system. Most of the present wind generator and power converter systems are based on the 690Vand two-level voltage–source or current–source converters are normally used [3], [4]. The continuous increase in wind turbine power ratings will generate larger current, e.g., from 1673 A for 2-MW system to 8810 A for 10-MW system. Power converters are therefore connected in parallel to handle the increasing current [5], [6]. Meanwhile, large current transfer results in a parallel connection of multiple power cables going down through the tower and causes substantial losses ( ), voltage drop, as well as high cost of cables, switchgears, and terminal connections [7]. These disadvantages can be offset by placing the step-up transformer (e.g., 690 V/33 kV) into the nacelle. However, the bulky and heavy transformer occupies the limited space of the nacelle and increases the mechanical stress of the tower. Therefore, a medium-voltage power conversion system (e.g., 10 kV) would be more desirable for large wind power conversion by reducing the current level and associated cable cost and losses, as well as improving the system power density. The benefits of adopting medium-voltage power conversion technology have been proved in motor drive applications, where medium-voltage (3–33 kV) configuration is generally used when the system power rating is higher than 1 MW [8]. Table I shows the current rating of an exemplar 5- and 10-MW systems with 690-V and 10-kV voltage level for comparison. As seen, transferring from low voltage

ISSN No: 2348-4845
International Journal & Magazine of Engineering, Technology, Management and Research
A Peer Reviewed Open Access International Journal

(690 V) to medium voltage (10 kV) can significantly reduce the current level. Further, considering the high maintenance cost and fault-tolerant requirement especially for offshore wind applications, a modular converter and generator structure is even preferable.

Regarding medium-voltage multilevel converter topologies for wind power applications, papers [9]–[12] investigate the suitability of three-level neutral-point-clamped converters. Although a higher voltage rating and reduced output harmonics are achieved, the ac-side voltage is limited to 4.0 kV if using 4.5-kV integrated gate-commutated thyristors (IGCTs) [11]. The voltage rating may be further increased if using 6-kV IGCT; however, the cost and availability becomes a major concern. A five-level hybrid converter topology with increasing number of devices is presented in [13] to further increase the converter voltage and power capability. However, the reliability restricts its application. If one device fails, the whole converter system operation may be interrupted. A more applicable way to achieve 6- or 10-kV medium-voltage power conversion is through the cascaded modular converter structure [2], [8]. The voltage level can be easily scaled up by cascading more converter cells. Papers [14]–[18] have proposed various converter topologies based on this concept. However, the fundamental connections between these topologies are not analyzed. The cascaded converter topology has intrinsic fault-tolerant operation capability. If one cell fails, it can be bypassed and the rest healthy cells can keep operation [17]. One of the main disadvantages of the cascaded

TABLE I
WIND TURBINE CURRENT RATING FOR DIFFERENT VOLTAGE LEVELS

Wind turbine power (MW)	Voltage (kV)	Current (A)
5.0	0.69	4400
	10	303
10	0.69	8810
	10	607

Converter topology is the large dc-link capacitor required to filter the dc-link voltage ripple from the H-bridge side in each cell [14], [19]. The dc-link capacitor is unreliable and is not favored in wind power applications where maintenance cost is very high. There are no effective solutions to significantly reduce the dc link capacitor. In motor drive applications, diode rectifiers are normally used, which cannot be actively controlled to compensate the ripple power thus reducing the dc-link capacitor.

In this paper, a fundamental rule to construct multilevel modular high power converters for large wind turbine power conversion is proposed. Based on this, three potential multilevel modular wind power converter topologies have been derived using a generalized approach for an exemplar 10-kV, 10-MW wind turbine. A special focus has been given to the topology comprising a 10-kV generator, a multilevel modular converter, and a multi-winding grid-side transformer. A solution to reduce the dc-link capacitor is proposed by compensating the ripple power from the three-phase grid-side inverter. A resonant controller is presented to achieve this purpose. The current harmonics induced in the inverter and transformer secondary windings by the proposed control scheme and their impact are also investigated analytically. The converter topology and dc-link capacitor reduction strategy has been simulated and validated with a 10-kV, 10-MW wind power conversion system, where the dc-link voltage ripple is effectively attenuated without affecting the grid power quality.

10-kV, 10-MW WIND POWER MODULARCONVERTER TOPOLOGIES

As mentioned, one of the most applicable and economic way to achieve a 10-kV power conversion system is through series connection of modular converter cells. In particular, 3.3-Kv insulated-gate bipolar transistor (IGBT) device is considered in this application due to their better availability and lower cost, compared with 4.5- and 6-kV devices. Fig. 1 shows a generalized phase leg of a cascaded modular converter structure. The outputs of several converter cells (ac/dc/ac) are connected in series to achieve high-voltage output. With 3.3-kV IGBTs, 10-kV line voltage output can be achieved with five stages, where each module dc-link voltage is regulated at around 1800 V, thus 3.3-kV devices can be used. It should be noted that the converter modules in Fig. 1 cannot be directly connected in series at both ends without

ISSN No: 2348-4845
International Journal & Magazine of Engineering, Technology, Management and Research
A Peer Reviewed Open Access International Journal

isolation. A galvanic isolation is needed in each converter module in order to cascade the outputs at either end. There are three possible locations to place the isolation, viz., at the generator side (I), in the dc link (II), or at the grid side (III), as shown in Fig. 1. The isolation can be achieved through either generator isolated windings, high-frequency transformer in the dc-link or multi-winding grid-side transformer. Based on this,

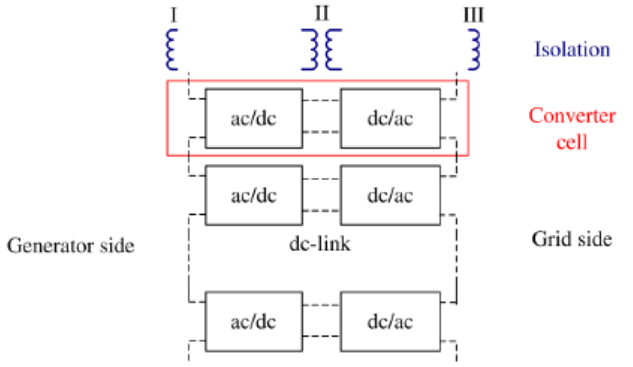

Fig.1. Generalized cascaded multilevel converter topology (one phase leg).

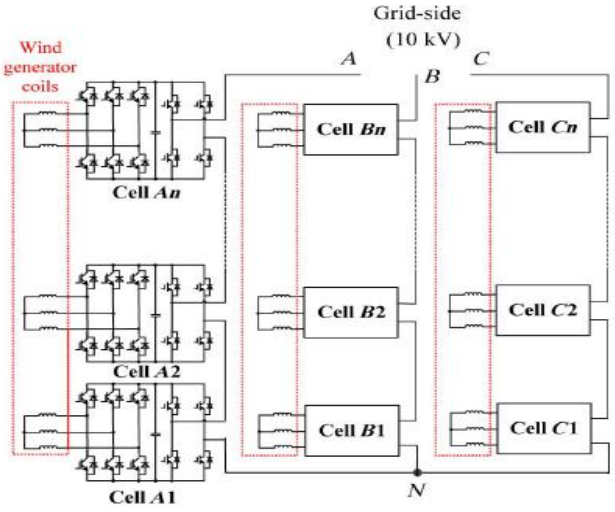

Fig.2. High-power, medium-voltage (10 kV) modular wind converter with generator-side isolation (converter type I).

three potential high-power, medium-voltage modular wind converter topologies are given in Figs. 2–4, respectively.

Fig. 2 shows a high-power, medium-voltage (10 kV) wind converter topology (type I) by using the generator-side isolation. The isolated coils in the generator stator windings are connected out separately to provide independent power sources for each converter cell. The input power stage of each cell is a three-phase active rectifier and the output stage is an H-bridge inverter. The outputs of each H-bridge are connected in series to achieve high voltage (e.g., 10 kV) at the grid side. This topology requires the generator to provide multiple three-phase coils. The direct-drive PMGs generally have many pole pairs, where the corresponding three-phase coils of each pole pair (or several pole pairs connected in series or in parallel, depending on the required voltage rating) can be connected out separately to meet this requirement. Regarding the control, the input three-phase rectifier is responsible for regulating the dc-link voltage of each converter cell and the grid-side cascaded H-bridge converter regulates the active power [e.g., for maximum power point tracking (MPPT)] and reactive power fed into the grid [14], [16]. With this topology, the generator and converter are suggested to put on top of the wind tower. A step-up transformer from 10 kV to the voltage level

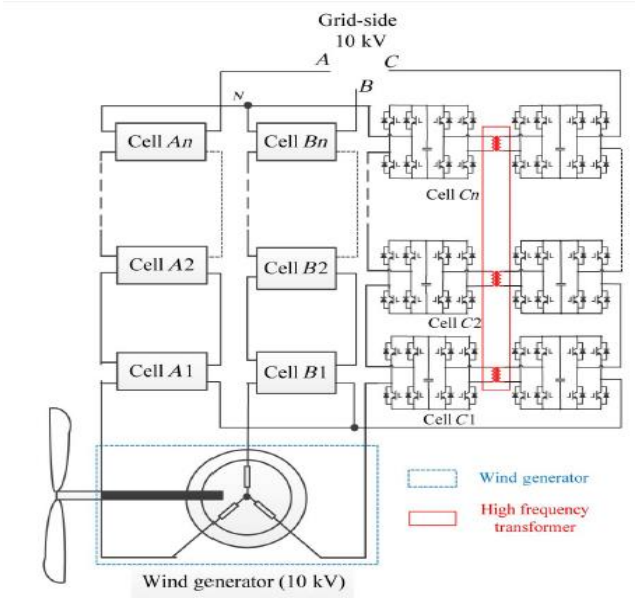

Fig.3. High-power, medium-voltage (10 kV) modular wind converter with high frequency transformer isolation (converter type II).

ISSN No: 2348-4845
International Journal & Magazine of Engineering, Technology, Management and Research
A Peer Reviewed Open Access International Journal

(e.g., 33 kV) of the collection point of the wind farm may be required and can be placed at the bottom of the tower. Alternatively, a transformer-less structure may be enabled if the number of cascaded stages can be increased to directly meet the collection point voltage. It should be noted that the increased number of generator terminal connections may add extra labor and maintenance cost. A dedicated generator design and wire connection arrangement may be required.

Fig. 3 shows a second wind converter topology (type II) with a high-frequency transformer as the isolation, which is inserted into the dc link together with a back-to-back H-bridge converter. This high-frequency isolation unit is also called dual active bridge (DAB) converter, where the two H-bridge converters at both sides of the high-frequency transformer operate at a higher frequency (e.g., several kHz), thus the size and weight of the transformer can be significantly reduced compared with the line frequency (50 or 60 Hz) transformer [20], [21].

The input and output stages of each converter cell are H-bridge converters (with the DAB converter in between). A standard three-phase 10-kV generator is used and the H-bridge converters are cascaded at both the generator side and grid side to achieve 10-kV voltage capability thus regulating the generator and grid power.

The turns ratio of the high-frequency isolation transformer can be adjusted (1:1 or 1: *n*) to achieve the desired voltage level. The power converter can be put flexibly either on top of the tower or at the bottom since 10-kV voltage is achieved at both ends of the converter. The main concern with this topology is the extra losses caused by the inserted DAB converter and high-frequency transformer, which may be mitigated by using advanced magnetic material, soft-switching topologies and new wide-bandgap power devices, e.g., silicon-carbide (Sic) based device.

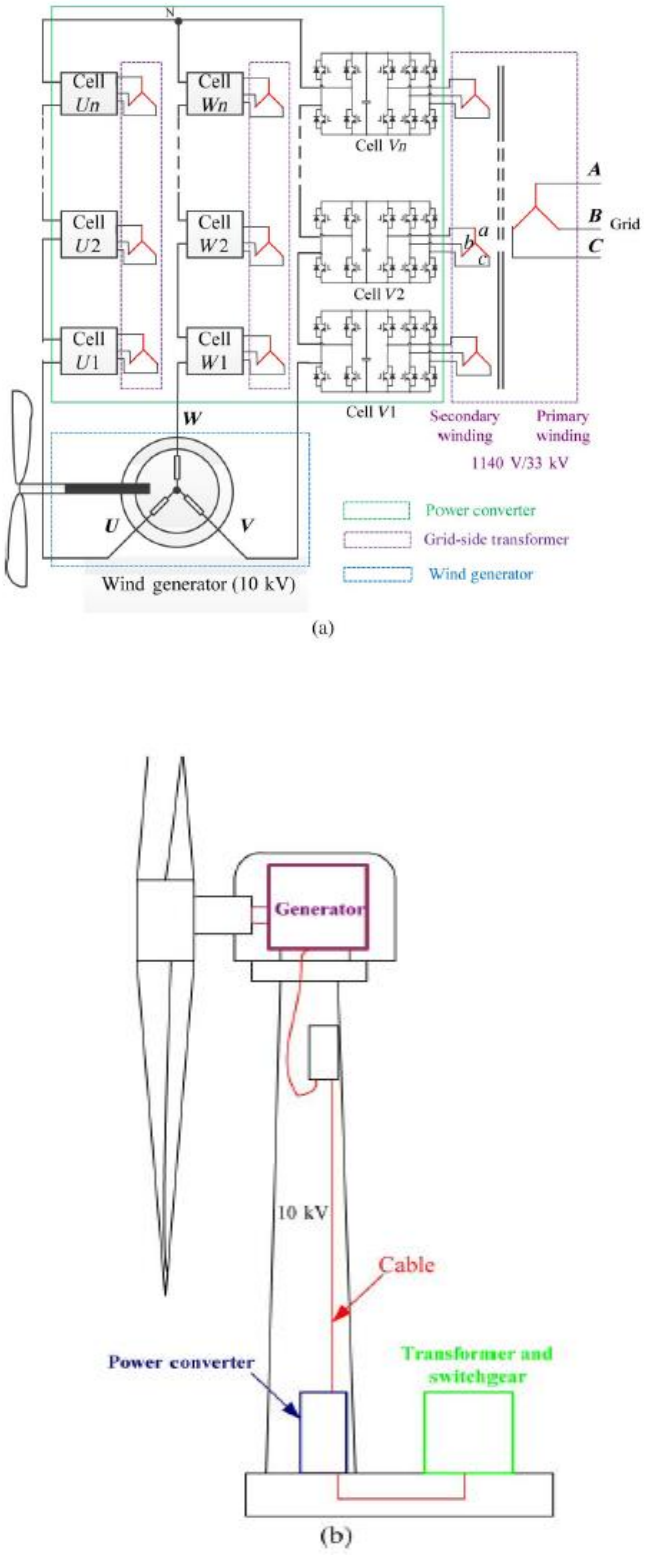

Fig.4. High-power, medium-voltage (10 kV) modular wind converter with grid side transformer isolation (converter type III): (a) generator and converter structure and (b) wind turbine electrical configuration.

ISSN No: 2348-4845
International Journal & Magazine of Engineering, Technology, Management and Research
A Peer Reviewed Open Access International Journal

Fig. 4(a) shows another high-power, medium-voltage wind converter topology (type III) with a grid-side isolation transformer, which will be further investigated in this paper. As can be seen, this topology adopts a standard 10-kV wind generator and a grid-side step-up transformer with multiple secondary windings (1140 V/33 kV), which provides isolation of each converter cell and also boosts the converter voltage to the grid voltage of 33 kV. The power converter and the transformer can be put at the bottom of the tower as shown in Fig. 4(b), which reduces the mechanical stress of the tower and saves the space in the nacelle. The input stage of each converter cell is an H-bridge rectifier which is then connected in series to achieve 10-kV voltage capability to control the generator. The output stage of each converter cell is a three phase inverter and is connected to the transformer secondary windings, responsible for regulating the dc-link voltage. Similar to the previous two topologies, this modular structure benefits from fault-tolerant capability, when one cell fails, it can be bypassed by a switch connected in parallel to the H-bridge converter output and the remaining health cells can still maintain operation subject to the reduce of power output. In view of the successful applications of the cascaded H-bridge converter in high power motor drive area, this topology may become a strong candidate for future large wind turbine power conversion systems [22].

It should be noted that the low-frequency single-phase fluctuating power at the input stage of each cell (H-bridge) in Fig. 4(a) will cause dc-link voltage ripple, which gets larger with lower generator stator frequency and higher power level. For variable speed, direct-drive PMGs, the stator frequency is generally low (e.g., below 15 Hz). Therefore, large dc-link capacitance is required to smooth out the voltage ripple appeared on the dc link, which are bulky and significantly increase the system cost as well as cause reliability issues due to the lifetime of electrolytic capacitors. This issue also happens to the other two topologies in Figs. 2 and 3. In Section IV, a solution to reduce the dc-link capacitance will be introduced in a later session.

10-MW WIND TURBINE SPECIFICATIONS AND CONVERTER

CONTROL STRATEGY

A. 10-MW Wind Turbine Specifications

A 10-kV, 10-MW wind turbine and its PMG parameters are designed. The rated speed of the wind turbine is 10 rpm at wind speed of 12 m/s [23]. The PMG has 90 pole pairs, corresponding to 15-Hz stator frequency at rated speed. Fig. 5 shows the captured wind power variation with the generator speed. The wind turbine control should aim to capture maximum wind power by regulating the generator speed/power following MPPT under normal conditions.

B. Generator and Cascaded H-Bridge Converter Control Strategy

The wind generator (PMG) shown in Fig. 4(a) can be modeled in a synchronous rotating (,) frame [3], [24]. With rotor flux oriented control, the PMG torque can be controlled by the –axis current, while the -axis current is controlled to maximize the generator efficiency. In order to achieve MPPT, the generator torque reference is set as the product of the optimal coefficient and the square of generator speed [25]. The standard phase shifted pulse width modulation (PWM) is adopted to modulate the cascaded H-bridge converters, thus generating the required voltage according to the voltage reference.

C. Grid-Side Inverter Model and Control Strategy

At the grid side, the three-phase inverter in each converter cell as shown in Fig. 4(a) is responsible for regulating the converter cell dc-link voltage, transferring the active power generated from wind generator to the grid. Since the inverter current is actively

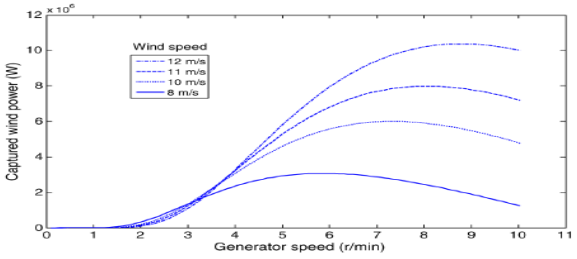

Fig.5. Variation of captured wind power with generator speed under different wind speeds.

ISSN No: 2348-4845
International Journal & Magazine of Engineering, Technology, Management and Research
A Peer Reviewed Open Access International Journal

controlled to be sinusoidal, the topology in Fig. 4(a) does not Need multiple phase-shifted transformer secondary windings (Zigzag winding) for harmonics reduction as the case in motor drive applications with diode rectifier, leading to a simplified transformer design. The transformer leakage inductance can be further used as the filter inductance. The model of the grid-side three-phase inverter in each cell on frame is given as follows [3], [14]:

$$\begin{cases} L_e \frac{di_d}{dt} = -R_e i_d + \omega_e L_e i_q - S_d + u_d \\ L_e \frac{di_q}{dt} = -R_e i_q - \omega_e L_e i_d - S_q + u_q \end{cases} \quad (1)$$

Where *Le* and *Re* are the transformer leakage inductance and resistance; *u*d, *uq*, *id*, *iq* are the voltages and currents on the transformer secondary side in the *d*, *q* frame, respectively; are the output voltages of the three-phase inverter in the switching average model; and ωe is the grid line frequency.

If the -axis of the rotating frame is aligned to the transformer secondary voltage vector, then *uq=0* and *u*d=E where E is the amplitude of the transformer secondary voltage. The converter active power P and Q reactive power can be formulated by

$$\begin{cases} P = \frac{3}{2}(u_d i_d + u_q i_q) = \frac{3}{2} E i_d \\ Q = \frac{3}{2}(u_d i_q - u_q i_d) = \frac{3}{2} E i_q. \end{cases} \quad (2)$$

As seen, the active and reactive power flowing into the grid can be controlled by -axis and -axis currents independently. The grid-side three-phase inverter control diagram is shown in Fig. 6. The outer loop is the dc-link voltage control loop which is kept to be 1800 V and inner loops are -axis and -axis current control loops. The -axis current can be used to provide reactive power to the grid when required subject to the current capability of the converter.

CONVERTER DC-LINK VOLTAGE RIPPLE REDUCTION

A. Resonant Controller Added in the Control Loop

One particular issue with the converter topology shown in Fig. 4(a) is the large dc-link capacitor required in each cell to smooth the single-phase pulsating power from the H-bridge (generator) side, which can be expressed as

$$\begin{aligned} p_{g\_single}(t) &= v_{o,U}(t) \cdot i_{o,U}(t) = V_{om}\cos(\omega_o t) \cdot I_{om}\cos(\omega_o t - \varphi) \\ &= \frac{V_{om} I_{om}}{2}\cos\varphi + \frac{V_{om} I_{om}}{2}\cos(2\omega_o t - \varphi) \\ &= P_{avg} \cdot \cos\varphi + P_{avg} \cdot \cos(2\omega_o t - \varphi) \end{aligned} \quad (3)$$

Where V_{om} and I_{om} are the amplitudes of the generator voltage (*u*o, u) and current (*Io*, *U*) seen at each cell, respectively. P_{avg} Is the average power flowing into the converter cell ωo is the generator stator frequency and φ is the generator power factor angle. As seen, the second term in (3) represents the pulsating power with the frequency of 2ωo, which causes dc-link voltage ripple. The amplitude of dc-link voltage ripple ΔV can be expressed as

$$\Delta V = \frac{P_{avg}}{\omega_o \cdot C \cdot V_{dc}} \quad (4)$$

Where C is the dc-link capacitor and Vdc is the dc-link voltage. As seen, the dc-link voltage ripple becomes larger with lower generator frequency and higher power rating. To keep the dc-link voltage ripple within ΔV, the required dc-link capacitance C can be calculated by

$$C \geq \frac{P_{avg}}{\omega_o \cdot \Delta V \cdot V_{dc}}. \quad (5)$$

For a 10-MW wind power converter with 15 cells (5 stages), 1800-V dc-link voltage, and 15-Hz generator stator frequency, the required capacitor in each cell will be 44 mF in order to keep the voltage ripple to be within 5% (90 V) at the rated operating point.

ISSN No: 2348-4845
International Journal & Magazine of Engineering, Technology, Management and Research
A Peer Reviewed Open Access International Journal

To achieve such large capacitance at this voltage level, many electrolytic capacitors need to be connected in both series and in parallel, which are not only expensive and bulky, but also cause reliability issues of the system, since the electrolytic capacitor has almost the highest failure rates in a typical wind power converter system [26]. For offshore applications, high reliability is a key to reduce the maintenance cost. Therefore, an effective method to reduce the required dc-link capacitor is critical. Due to the use of controlled three-phase inverter in each cell, the power transferred to the transformer secondary winding can be well adjusted to compensate the power ripple from the H-bridge rectifier. If the power of the three-phase inverter in (2) is regulated the same as the power from the H-bridge rectifier as in (3) (including the pulsating power), in theory, no dc-link capacitor is required to handle the low-frequency (2ωo) power ripple.

By equating (2) with (3), the inverter -axis current becomes (6) under vector control

$$\begin{cases} i_{d,U} = \frac{V_{om} I_{om}}{3E} [\cos\varphi + \cos(2\omega_o t - \varphi) \\ i_{q,U} = 0 \end{cases} \quad (6)$$

Where *id*,U and *iq,U* are -axis and -axis currents assuming that the three-phase inverter is connected to phase *U* of the generator. As can be seen, the -axis current has an ac component with the

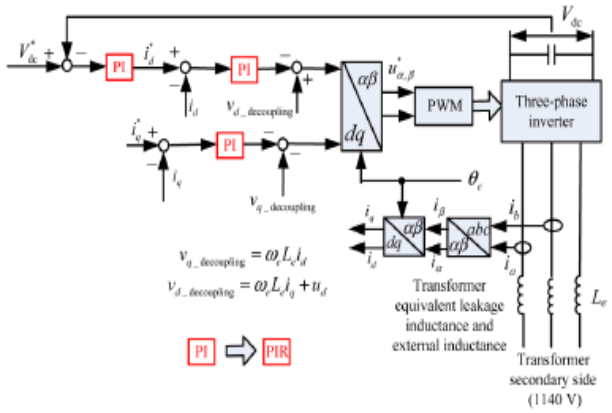

Fig.6. Vector control diagram of the grid-side inverter in each cell (The PI controller is replaced with a PIR controller when the dc-link voltage ripple reduction function is enabled.).

Frequency 2ωo of, which is different from the conventional control where only dc component exists.

If the -axis current of the three-phase inverter can be controlled the same as in (6), then there will be no dc-link low frequency voltage ripple in steady state. However, the conventional proportional–integral (PI) controllers used in standard dc-link voltage and current loops in Fig. 6 can only guarantee zero steady-state error for dc component, not at twice of the generator stator frequency (2ωo). Therefore, a proportional–integral–resonant (PIR) controller is introduced here to replace the PI controller thus regulating the pulsating power 2ωo at frequency. The resonant frequency of R-controller is set at 2ωo. The transfer function of the PIR controller is given as follows [27], [28]:

$$G_{\mathrm{PIR}}(s) = K_p + \frac{K_i}{s} + \frac{2K_r s}{s^2 + (2\omega_o)^2} \quad (7)$$

Where KP, K*i*, and are the proportional, integral, and resonant coefficients, respectively.

The selection of KP and K*i* will follow the standard current loop design process to achieve a desirable control bandwidth. Based on the grid-side inverter model in (1), the -axis current loop plant model can therefore be expressed as

$$\frac{I_d(s)}{S_d(s)} = \frac{1}{sL_e + R_e} \quad (8)$$

Where $\omega_e L_e i_q$ and u_d are treated as cross-coupling terms. If K_p is chosen as $\omega_c L_e$ and K_i is chosen as $\omega_c R_e$, where ω_c is the designed current-loop bandwidth, the closed-loop transfer function will become

$$\frac{I_d^*(s)}{I_d(s)} = \frac{\omega_c}{s + \omega_c}. \quad (9)$$

ISSN No: 2348-4845
International Journal & Magazine of Engineering, Technology, Management and Research
A Peer Reviewed Open Access International Journal

It can be seen that the closed-loop transfer function is a first order system with a bandwidth of ω_c . The -axis current-loop diagram is shown in Fig. 7.

The selection of *Kr* is to make sure that there is sufficient gain at the resonant frequency to reduce the low-frequency current ripple. In theory, since the resonant controller has infinite gain at

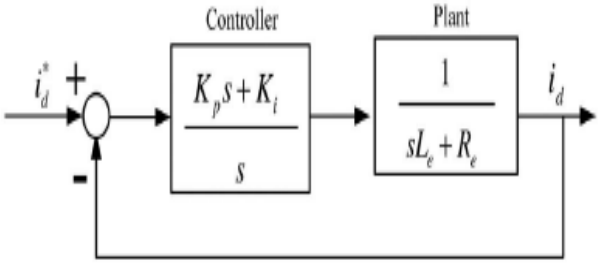

Fig.7. Current-loop diagram with a PI controller

the resonant frequency, *Kr* can be any positive value (e.g., *Kr* > 1). However, in digital implementation, due to discretization effect, the gain at the resonant frequency may be limited. Therefore, a larger *Kr* value is preferred. It should also be noted that if the *Kr* value is too large, the stability of the system may be affected especially when the resonant frequency is close to the current-loop cross-over frequency.

Fig. 8 shows the open-loop and closed-loop frequency domain response of using PI and PIR controllers for comparison. The current-loop bandwidth $\omega_c = 300$ Hz, $R_e = 0.01\ \Omega, L_e = 1$ mH, therefore, KP= 0.3, Ki = 3 the resonant frequency $2\omega_o$ = 100Hz and *Kr=100*.

As seen, the resonant (R) controller creates an infinite gain at the resonant frequency (100 Hz). In the closed loop, this converts to unity gain and zero phase delay at the resonant frequency, which means the real current can follow the reference accurately. Therefore, the ripple power can be effectively compensated and the dc-link voltage ripple is reduced. The design of the PIR controller for the voltage loop can follow the same process.

In addition, considering the accuracy of the generator Frequency /speed measurement, it is desirable to have a certain tolerance

when setting the resonant frequency. Therefore, a band pass controller/filter can be used, instead of the pure resonant controller. This will improve the robustness of the controller especially when there is small error in the frequency measurement. The band pass controller will also avoid the stability issues caused by the infinite gain of the resonant controller at the resonant frequency. The transfer function of the band pass filter is given as follows:

$$G_{R\_BP} = \frac{2K_r\omega_b s}{s^2 + 2\omega_b s + \omega_o^2} \quad (10)$$

Where is ωo the center frequency of the band pass filter and ωb is the bandwidth of the band pass filter. The band pass filter has a high, but limited gain at the resonant frequency ωo, which can be further tuned by the resonant gain *Kr*.

Note that the resonant frequency varies with the generator frequency/speed. Therefore, the generator frequency information needs to be fed to the PIR controller to set the resonant frequency.

It should also be noted that on using this dc-link voltage ripple reduction scheme, the power transferred to the transformer secondary winding in each cell will contain a power ripple, instead of a constant power. As a result, the three-phase inverter current (transformer secondary-winding current) is not sinusoidal and contains harmonics.

However, these current harmonics are canceled with each other among the transformer secondary windings and do not appear at the transformer primary-side/ grid-side (33 kV) and therefore would not affect the grid power

ISSN No: 2348-4845
International Journal & Magazine of Engineering, Technology, Management and Research
A Peer Reviewed Open Access International Journal

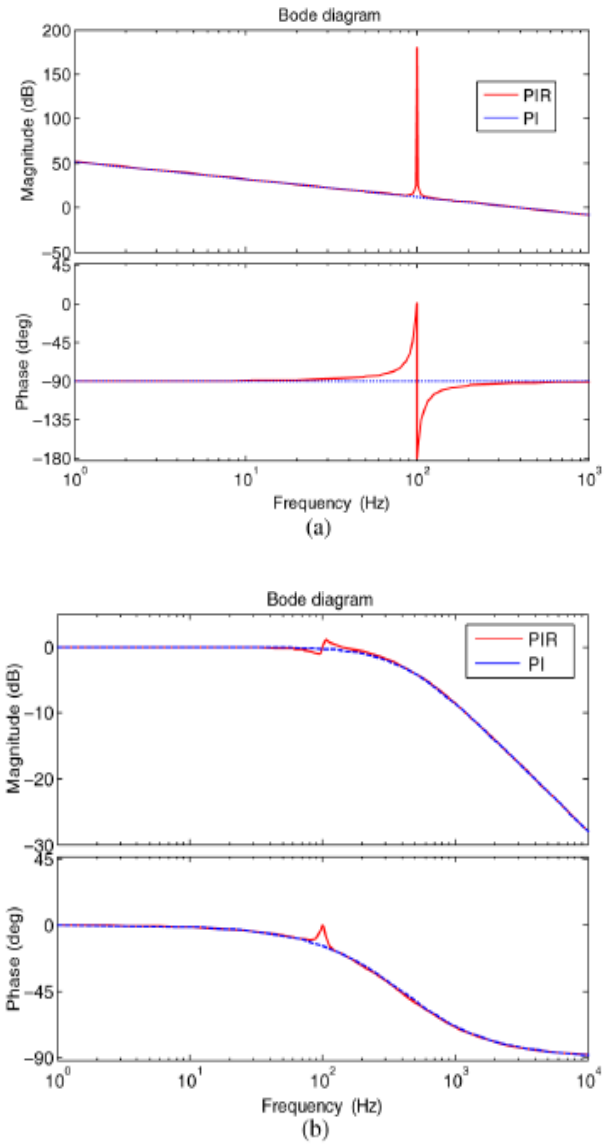

Fig. 8. Current-loop frequency response with PI and PIR controllers: (a) open loop frequency response and (b) closed-loop frequency response.

Quality. Section IV-B will analyze the current harmonics in both the transformer secondary and primary windings.

B. Current Harmonics Analysis

In the following analysis, the generator phases are denoted by *A, U, V, W,* and the transformer primary phases are denoted by A, B, C and the transformer secondary phases are denoted by a, b ,c , respectively, as indicated in Fig. 4(a).

Connecting to the cells of generator phase *U* is given. Similarly, the corresponding -axis current of the three-phase inverters of the cells connected to generator phases *V* and *W* can be derived as in (11) and (12) by considering the phase shift of 120

$$i_{d,V} = \frac{V_{om} I_{om}}{3E}\left[\cos\varphi + \cos\left(2\omega_o t - \varphi - \frac{4\pi}{3}\right)\right] \quad (11)$$

$$i_{d,W} = \frac{V_{om} I_{om}}{3E}\left[\cos\varphi + \cos\left(2\omega_o t - \varphi + \frac{4\pi}{3}\right)\right]. \quad (12)$$

To analyze the current harmonics in the three-phase inverter, the , currents given in (6), (11), and (12) are transformed back to , , coordinate by using inverse-Park transformation. For the cells connecting to phase *U* of the generator, the inverter phase *a* current (transformer secondary current) can be expressed as

$$\begin{aligned} i_{a,Ui} &= \frac{V_{om} I_{om}}{3E}[\cos\varphi + \cos(2\omega_o t - \varphi)]\cos(\omega_e t + \theta_{0,Ui}) \\ &= \frac{V_{om} I_{om}}{3E}\left\{\begin{array}{l} \cos(\omega_e t + \theta_{0,Ui})\cos\varphi \\ +\frac{1}{2}\cos[(\omega_e + 2\omega_o)t + (\theta_{0,Ui} - \varphi)] \\ +\frac{1}{2}\cos[(\omega_e - 2\omega_o)t + (\theta_{0,Ui} + \varphi)] \end{array}\right\} \end{aligned} \quad (13)$$

where *ia,Ui* represents the phase current of the inverter and the suffix *U* denotes the inverter cell which is connected to phase *U* of the generator. Suffix *i* denotes the *i*th module of the module string.θ0, *Ui* is the phase angle of the transformer secondary voltage ωe and is the grid frequency. As seen from (13), the inverter phase current (transformer secondary current) contains not only the fundamental component with the grid frequency of ωe , but also the frequency components ωe + 2ωo of and ωe - 2ωo . These current harmonics are due to the compensation of the power ripple from the H-bridge side.

Similarly, the inverter phase current of the cells connected to generator phases V and W can be expressed as in (14) and (15), respectively,

ISSN No: 2348-4845
International Journal & Magazine of Engineering, Technology, Management and Research
A Peer Reviewed Open Access International Journal

$$i_{a,Vi}=\frac{V_{om}I_{om}}{3E}\left\{\begin{array}{l}\cos(\omega_e t+\theta_{0,Vi})\cos\varphi\\ +\frac{1}{2}\cos\left[(\omega_e+2\omega_o)t+\left(\theta_{0,Vi}-\varphi-\frac{4\pi}{3}\right)\right]\\ +\frac{1}{2}\cos\left[(\omega_e-2\omega_o)t+\left(\theta_{0,Vi}+\varphi+\frac{4\pi}{3}\right)\right]\end{array}\right\} \quad (14)$$

$$i_{a,Wi}=\frac{V_{om}I_{om}}{3E}\left\{\begin{array}{l}\cos(\omega_e t+\theta_{0,Wi})\cos\varphi\\ +\frac{1}{2}\cos\left[(\omega_e+2\omega_o)t+\left(\theta_{0,Wi}-\varphi+\frac{4\pi}{3}\right)\right]\\ +\frac{1}{2}\cos\left[(\omega_e-2\omega_o)t+\left(\theta_{0,Wi}+\varphi-\frac{4\pi}{3}\right)\right]\end{array}\right\} \quad (15)$$

Where θ0, θ0Wi are the voltage phase angles of the transformer secondary windings of the cells connected to the generator phases V, W, respectively. In the converter and transformer configuration shown in Fig. 4(a), all the transformer secondary voltages have the same phase angle with respect to the primary side .Therefore, $\theta_{0,Ui}=\theta_{0,Vi}=\theta_{0,Wi}=\theta_{0,i}$

If the inverter phase *a* currents of the cells connected to generator phases *U*, *V*, *W*, as shown in (13)–(15), are added together, the total phase current becomes

$$i_{a,Ui}+i_{a,Vi}+i_{a,Wi}=\frac{V_{om}I_{om}}{E}\cos(\omega_e t+\theta_{0,i})\cos\varphi. \quad (16)$$

As seen, the harmonic currents with the frequency of ωe + 2ωo and ωe - 2ωo in each cell are canceled among the transformer secondary side. Therefore, they do not exist in the transformer primary. The transformer primary side (grid side) only contains the fundamental sinusoidal component with the frequency of ωe. The same current harmonics analysis can be done for phases and *b*. Therefore, the proposed dc-link capacitance reduction method does not affect the grid power quality, although the transformer secondary-side (inverter) will have current harmonics of ωe + 2ωo and ωe - 2ωo.

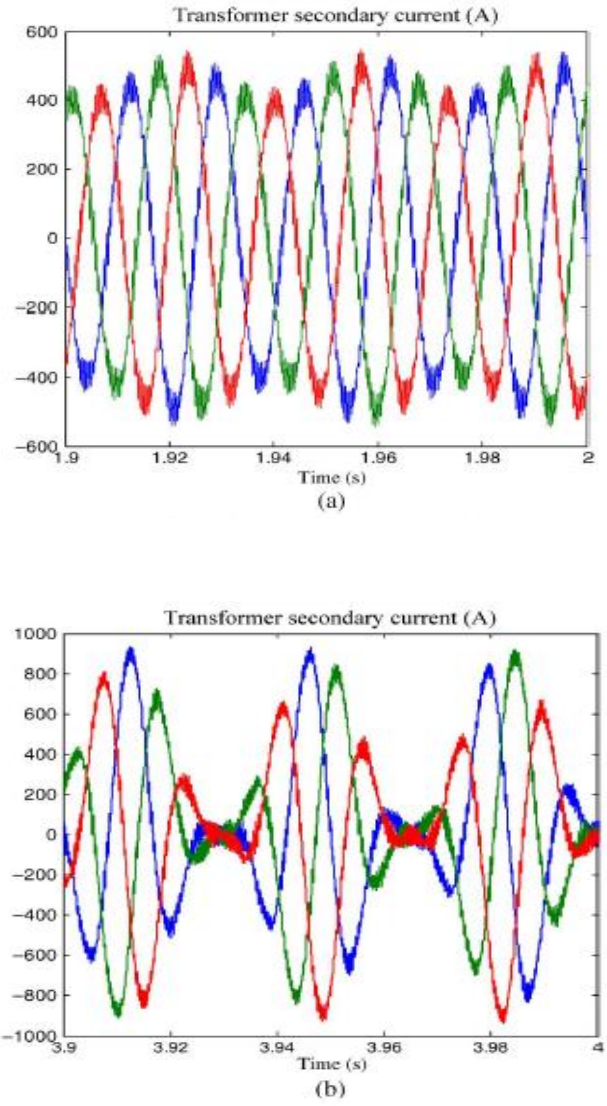

Fig.9. Inverter (transformer secondary) current with and without resonant controller applied: (a) without resonant controller and (b) with resonant controller.

C. Inverter and Transformer Power Losses Analysis

While the low-frequency power ripple from H-bridge side can be effectively compensated from the transformer-side inverter, the harmonic current may cause extra thermal stress to the inverter power devices and the transformer secondary windings. Fig. 9 shows the simulated inverter current waveform with and without the dc-link voltage ripple reduction method applied for a 10-MW system at a rated wind speed. As seen, with the dc-link ripple reduction method applied,

ISSN No: 2348-4845
International Journal & Magazine of Engineering, Technology, Management and Research
A Peer Reviewed Open Access International Journal

the peak current (due to the harmonics) of each phase may double the value of the current without compensation. The exact expression of the current waveform is given in (13)–(15) for phase. Therefore, the power device current rating should be chosen to meet the peak current requirement.

In order to evaluate the thermal performance and the impact of the control algorithm on the inverter, the inverter losses and device junction temperature are calculated and simulated. For a 10-MW, 10-kV generator, the rated root mean square (RMS) current is 577 A. With a 1140-V/33-kV grid-side transformer and

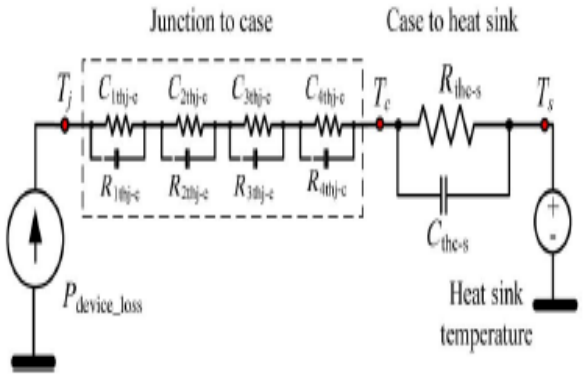

Fig.10. Thermal network to evaluate the device junction temperature.

15 converter cells, the transformer secondary winding RMS current is 337 A. Note that if the ripple power compensation scheme is activated, the peak of transformer secondary current may increase to 950 A. With these current values, IGBT modules from Infineon FZ1000R33HL3 (3300 V, 1000 A) are used for both H-bridge rectifier and the inverter to evaluate the system thermal performance [29], [30]. The switching frequency is selected at 2 kHz.

In the simulation, the heat sink temperature is assumed to be fixed at 80°C due to its large thermal time constant. The thermal network is shown in Fig. 10. The thermal network comprises the junction to case and case to heat sink thermal impedance.

Fig. 11 shows the inverter device junction temperature variation. Without ripple power compensation, the IGBT temperature varies between 96 and 102°C . The diode junction temperature varies between 94.5 and 104°C . When the ripple power compensation scheme is applied, the inverter current becomes as in Fig. 9(b) and the junction temperature variation gets larger as well as the peak temperature, although the average temperature stays similar with the non-compensated case. Larger junction temperature variation may reduce the lifetime of the power device. The thermal design should also make sure the peak temperature does not exceed the maximum allowable junction temperature.

Another impact of the ripple power compensation scheme is the circulating harmonic current inside the transformer secondary windings and the corresponding extra copper losses it has introduced. From (13), the RMS value of the transformer secondary current with harmonics can be calculated as

$$I'_{a\_RMS} = \frac{V_{om} I_{om}}{3E} \cdot \sqrt{\left(\frac{1}{\sqrt{2}}\right)^2 + \left(\frac{1}{2\sqrt{2}}\right)^2 + \left(\frac{1}{2\sqrt{2}}\right)^2} = \frac{V_{om} I_{om}}{3E} \cdot \frac{\sqrt{3}}{2} \quad (17)$$

Where I'*a*_RMS is the RMS value of the current including harmonics. The RMS value of the fundamental current can be calculated as

$$I_{a\_RMS} = \frac{V_{om} I_{om}}{3E} \cdot \frac{1}{\sqrt{2}}. \quad (18)$$

Therefore, the ratio of the transformer secondary copper loss with and without the ripple power compensation scheme can be calculated as

$$\left(\frac{I'_{a\_RMS}}{I_{a\_RMS}}\right)^2 = \left(\frac{\sqrt{6}}{2}\right)^2 = 1.5. \quad (19)$$

ISSN No: 2348-4845
International Journal & Magazine of Engineering, Technology, Management and Research
A Peer Reviewed Open Access International Journal

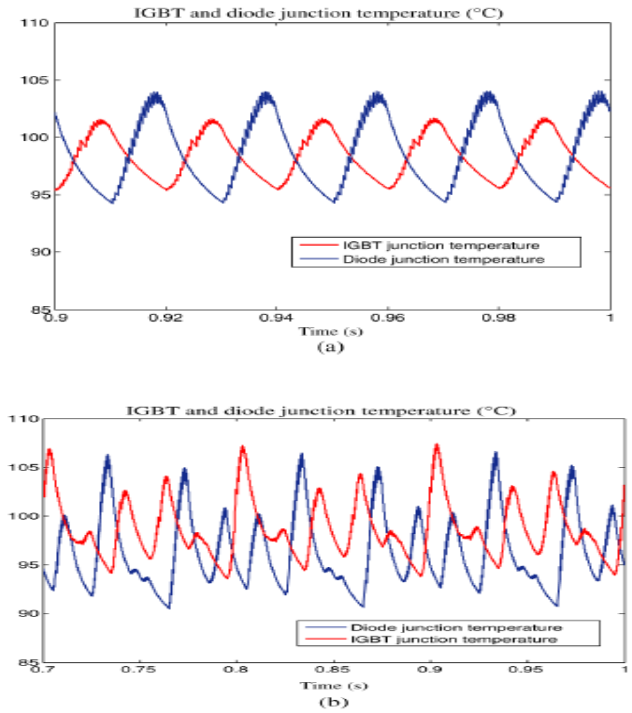

Fig.11. Inverter device (IGBT/diode) junction temperature variation: (a) without resonant controller and (b) with resonant controller.

As seen, the winding copper losses have increased by 50% due to the extra harmonics, which need to be taken into consideration during the transformer and cooling system design.

SIMULATION AND RESULTS

A simulation model has been built in MATLAB/Simulink in order to validate the converter topology in Fig. 4 and control strategy in Fig. 6. The power converter consists of 5 stages (15 cells), with each dc-link voltage of 1800 V. The dc-link capacitance is 44 mF. The wind turbine characteristics are the same as in Fig. 5.

Fig. 12 shows the steady-state simulation results at the wind speed of 12 m/s with 10-MW wind power generation. Fig. 12(a) shows the generator-side converter output voltage, which has 11 levels and the generator current. Fig. 12(b) shows the transformer secondary winding (inverter) currents (1140-V side) in one converter cell. The grid (33 kV) phase

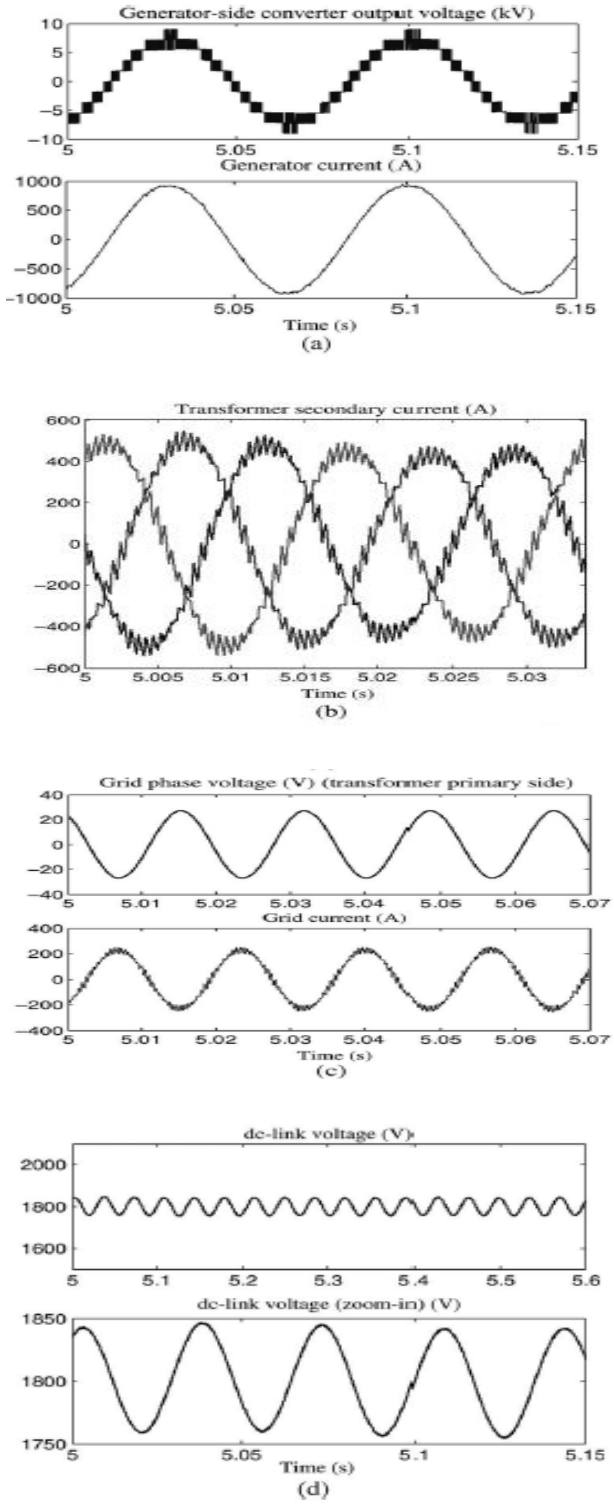

Fig. 12. Steady-state simulation results at wind speed of 12 m/s: (a) generator side converter output voltage and generator current, (b) transformer secondary winding current in a converter cell, (c) grid phase voltage and current, and (d) dc-link voltage and detailed trace.

ISSN No: 2348-4845
International Journal & Magazine of Engineering, Technology, Management and Research
A Peer Reviewed Open Access International Journal

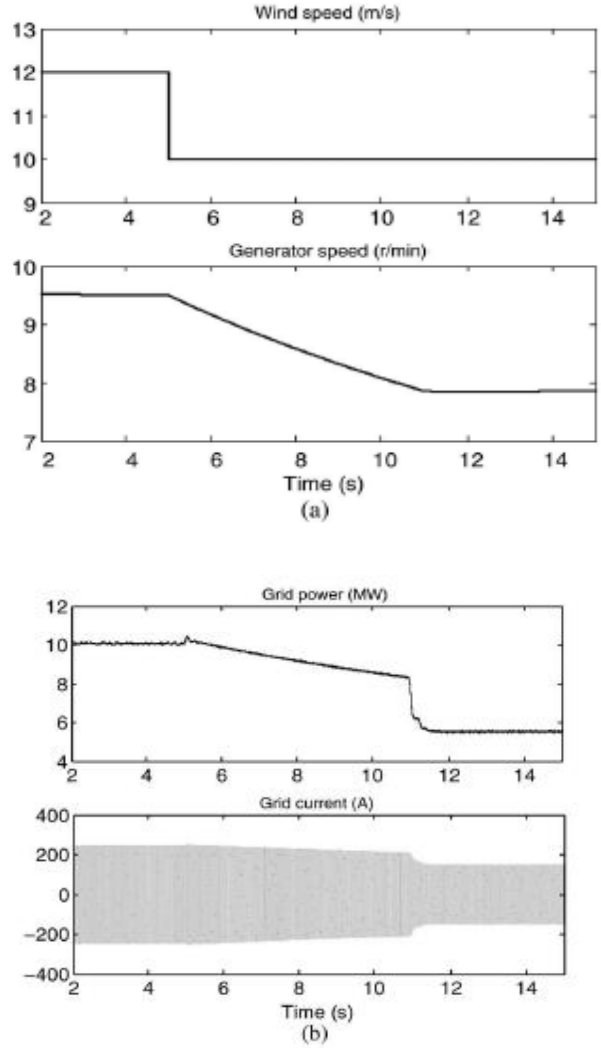

Fig.13. System response during wind speed drop from 12 to 10 m/s: (a) wind speed and generator speed and (b) power transferred to the grid and grid current.

Voltage and current are shown in Fig. 12(c). As seen, the grid current is kept sinusoidal and the phase relationship between voltage and current indicates wind power is fed into the grid. Fig. 12(d) shows the dc-link voltage regulated at 1800 V. With 44-mF dc-link capacitor, the voltage ripple is around 90 V, which agrees with the calculated results by (4). A detailed waveform is shown at the bottom of this figure and the ripple frequency is 30 Hz, which is twice of the generator frequency of 15 Hz.

Fig. 13 shows the system response during a wind speed drop from 12 to 10 m/s at 5 s. The converter and generator control aims to achieve MPPT under both wind speeds. Fig. 13(a) shows the wind speed profile and the corresponding generator speed. As seen, the generator speed reduces from 9.5 (MPPT point for 12 m/s) to 7.7 r/min to reach the MPPT point according to Fig. 5. Fig. 13(b) shows the power transferred to the grid and the grid current.

Fig. 14 shows the results of dc-link voltage ripple reduction by using the PIR controller in the dc-link voltage and current control loops of each converter cell, as illustrated in the diagram in Fig. 6. To observe the effect more clearly, the dc-link capacitance has been reduced from 44 to 22 mF. Therefore, without using PIR controller, the dc-link voltage ripple of each cell should be 180 V. Fig. 14(a) shows the dc link voltage, where the resonant controller is applied at 2 s. As

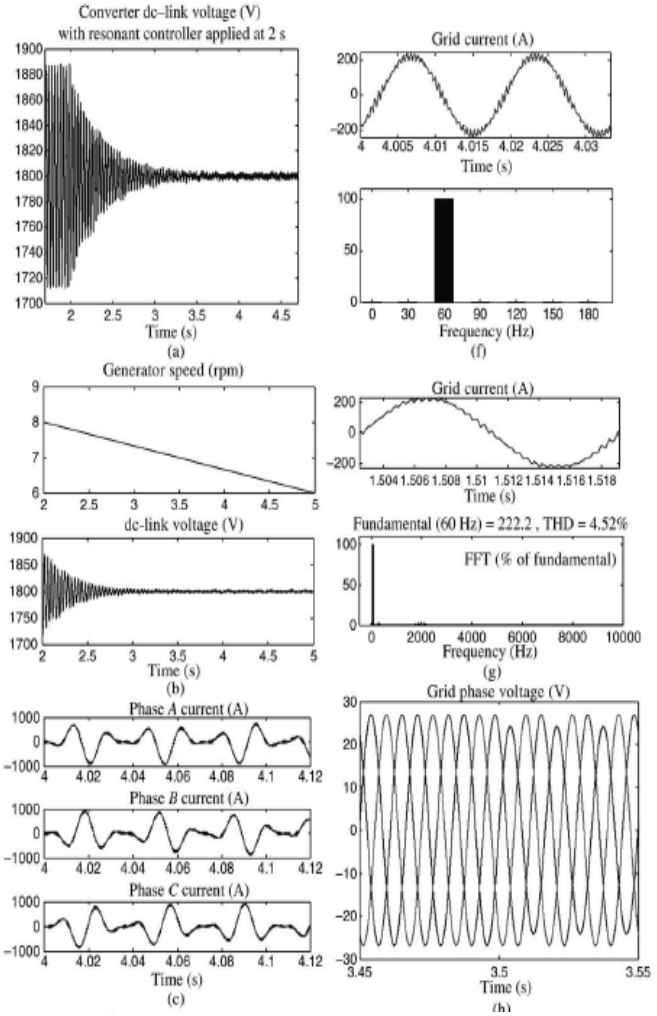

ISSN No: 2348-4845
International Journal & Magazine of Engineering, Technology, Management and Research
A Peer Reviewed Open Access International Journal

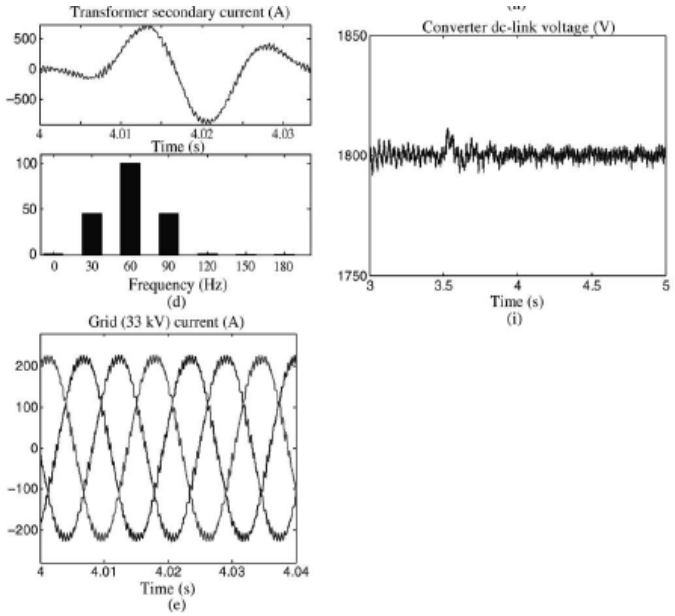

Fig. 14. Simulation results with a PIR controller engaged to reduce the dc-link voltage ripple: (a) converter cell dc-link voltage with resonant controller applied at 2 s, (b) dc-link voltage during generator speed variation, (c) transformer secondary winding current, (d) FFT analysis of transformer secondary winding current, (e) transformer primary (grid) current, (f) FFT analysis of transformer primary winding current, (g) THD of the grid current, (h) grid phase voltages with phase *A* 10% drop at 3.5 s, and (i) converter dc-link voltage under unbalanced grid.

Seen, before the resonant controller is applied, the dc-link voltage ripple is around 180 V. After the resonant controller is applied, the dc-link voltage ripple reduces dramatically to around zero, which validates the proposed dc-link voltage ripple reduction method. As a result, the required dc-link capacitor can be much smaller than that without a resonant controller, which can save the capacitor cost, size, as well as increase the system reliability. Fig. 14(b) further shows the performance of the controller during the change of generator speed. The resonant controller is applied at 2 s. During 2–5 s the generator speed varies from 8 to 6 rpm and the controller effectively adjusts the resonant frequency and attenuates the voltage ripple regardless of the generator speed variation. Fig. 14(c) shows the corresponding transformer secondary current in each cell when the resonant controller is engaged. As seen, the currents are not sinusoidal due to the compensation of the pulsation power. As analyzed in (13)–(15), the current contains harmonics with frequency of ωe + 2ωo and ωe-2ωo. The fast Fourier transform (FFT) analysis of the current is shown in Fig. 14(d), where the current contains the grid-frequency (ωe) component of 60 Hz as well as two other frequency components of 90 Hz (ωe + 2ωo) and 30 Hz ( ) at the generator stator frequency (ωe - 2ωo) of 15 Hz. Fig. 14(e) shows the transformer primary (grid)-side current waveform, which is sinusoidal and does not contain any low-frequency harmonics as indicated by the FFT analysis in Fig. 14(f) that only the 60-Hz grid-frequency component appears. It is evident that the proposed dc-link voltage ripple reduction method does not affect the grid-side power quality. Fig. 14(g) shows the total harmonic distortion (THD) of the grid current, which is 4.52% in this case, where the grid-interface inductance is 0.5 mH and the switching frequency is 2 kHz. Fig. 14(h) and (i) shows the effectiveness of the dc-link voltage ripple reduction scheme under an unbalanced grid condition. At 3.5 s, phase *A* voltage has a 10% voltage drop. From the converter dc-link voltage, it can be seen that the dc-link voltage ripple is effectively attenuated regardless the voltage drop in phase *A*.

CONCLUSION

In this paper, three high-power medium-voltage (10 kV) modular wind power converter topologies have been derived based on a generalized structure by using different formats of isolation. A method has been proposed to attenuate the dc-link voltage ripple, thus reducing the capacitor requirement, by compensating the low-frequency power ripple. A PIR

Controller-based control loop has been designed to achieve this purpose. The proposed dc-link voltage reduction scheme will introduce harmonics in the transformer secondary current; however, not degrading the grid power quality (sinusoidal current). The current harmonics will increase the stress of the power devices and the transformer copper loss. Simulation results with a 10-kV, 10-MW system have validated the converter topology and control scheme. The proposed

ISSN No: 2348-4845
International Journal & Magazine of Engineering, Technology, Management and Research
A Peer Reviewed Open Access International Journal

dc-link voltage ripple reduction method may also be used in the other two topologies presented in the paper.

ACKNOWLEDGMENT

The author would like to thank Dr. D. Grant, Visiting Fellow at the University of Bristol, for his comments on the paper.

REFERENCES

[1] M. Liserre, R. Cardenas, M. Molinas, and J. Rodriguez, "Overview of multi- MW wind turbines and wind parks," IEEE Trans. Ind. Electron., vol. 58, no. 4, pp. 1081–1095, Apr. 2011.

[2] F. Blaabjerg, M. Liserre, and K. Ma, "Power electronics converters for wind turbine systems," IEEE Trans. Ind. Appl., vol. 48, no. 2, pp. 708–719, Mar. 2012.

[3] M. Chinchilla, S. Arnaltes, and J. Burgos, "Control of permanent-magnet generators applied to variable-speed wind-energy systems connected to the grid," IEEE Trans. Energy Convers., vol. 21, no. 1, pp. 130–135, Mar. 2006.

[4] J. Dai, D. Xu, and B. Wu, "A novel control scheme for current–source– converter-based PMSG wind energy conversion systems," IEEE Trans. Power Electron., vol. 24, no. 4, pp. 963–972, Apr. 2009.

[5] J. Birk and B. Andresen, "Parallel-connected converters for optimizing efficiency, reliability and grid harmonics in a wind turbine," in Proc. EPE'07 Conf., Aalborg, Denmark, Sep. 2007, pp. 1–7.

[6] Z. Xu, R. Li, H. Zhu, D. Xu, and C. H. Zhang, "Control of parallel multiple converters for direct-drive permanent-magnet wind power generation systems," IEEE Trans. Power Electron., vol. 27, no. 3, pp. 1250–1270, Mar. 2012.

[7] W. Erdman and M. Behnke, "Low wind speed turbine project phase II: The application of medium-voltage electrical apparatus to the class of variable speed multi-megawatt low wind speed turbines," San Ramon, CA, USA, Natl. Renew. Energy Lab. Rep., NREL/SR-500-38686, Nov. 2005.

[8] H. Abu-Rub, J. Holtz, J. Rodriguez, and G. Baoming, "Medium-voltage multilevel converters-state of the art, challenges and requirements in industrial applications," IEEE Trans. Ind. Electron., vol. 57, no. 8, pp. 2581–2596, Aug. 2010.

[9] R. C. Portillo, M. M. Prats, J. I. Leon, J. A. Sanchez, J. M. Carrasco, E. Galvan et al., "Modelling strategy for back-to-back three-level converters applied to high-power wind turbines," IEEE Trans. Ind. Electron., vol. 53, no. 5, pp. 1483–1491, Oct. 2006.

[10] E. J. Bueno, S. Cóbreces, F. J. Rodríguez, A. Hernández, and F. Espinosa, "Design of a back-to-back NPC converter interface for wind turbines with Squirrel-cage induction generator," IEEE Trans. Energy Convers., vol. 23, no. 3, pp. 932–945, Sep. 2008.

[11] A. Faulstich, J. K. Steinke, and F. Wittwer, "Medium voltage converter for permanent magnet wind power generators up to 7 MW," in Proc. EPE Conf., Barcelona, Spain, Sep. 2009, pp. 9–17.

[12] C. L. Xia, X. Gu, and Y. Yan, "Neutral-point potential balancing of three level inverters in direct-driven wind energy conversion system," IEEE Trans. Energy Convers., vol. 26, no. 1, pp. 18–29, Mar. 2011.

[13] M. Winkelnkemper, F. Wildner, and P. K. Steimer, "6 MVA five-level hybrid converter for wind power," in Proc. IEEE PESC'08 Conf., Rhodes, Greece, Jun. 2008, pp. 4532–4538.

[14] X. Yuan, J. Chai, and Y. Li, "A transformer-less high-power converter for large permanent magnet wind generator systems," IEEE Trans. Sustain. Energy, vol. 3, no. 3, pp. 318–329, Jul. 2012.

ISSN No: 2348-4845
International Journal & Magazine of Engineering, Technology, Management and Research
A Peer Reviewed Open Access International Journal

[15] C. Xia, Z. Wang, T. Shi, and Z. Song, "A novel cascaded boost chopper for the wind energy conversion system based on the permanent magnet synchronous generator," IEEE Trans. Energy Convers., vol. 28, no. 3, pp. 512–522, Sep. 2013.

[16] C.H. Ng,M. A. Parker, R. Li, P. J. Tavner, J. R. Bumby, and E. Spooner, "A multilevel modular converter for a large light weight wind turbine generator," IEEE Trans. Power Electron., vol. 23, no. 3, pp. 1062–1074, May 2008.

[17] M. A. Parker, C. H. Ng, and L. Ran, "Fault-tolerant control for a modular generator converter scheme for direct drive wind turbines," IEEE Trans. Ind. Electron., vol. 58, no. 1, pp. 305–315, Jan. 2011.

[18] J. Kang, N. Takada, E. Yamamoto, and E. Watanabe, "High power matrix converter for wind power generation applications," in Proc. ICPE ECCE Asia Conf., Jeju, Korea, Jun. 2011, pp. 1331–1336.

[19] M. A. Perez, J. R. Espinoza, J. R. Rodriguez, and P. Lezana, "Regenerative medium voltage AC drive based on a multicell arrangement with reduced energy storage requirements," IEEE Trans. Ind. Electron., vol. 52, no. 1, pp. 171–180, Feb. 2005.

[20] S. Inoue and H. Akagi, "A bidirectional isolated dc–dc converter as a core circuit of the next-generation medium-voltage power conversion system," IEEE Trans. Power Electron., vol. 22, no. 2, pp. 535–542, Mar. 2007.

[21] F. Iov, F. Blaabjerg, J. Clare, O. Wheeler, A. Rufer, and A. Hyde, "UNIFLEX-PM-A key-enabling technology for future European electricity networks," EPE J., vol. 19, no. 4, pp. 6–16, 2009.

[22] J. Rodriguez, S. Bernet, B. Wu, J. O. Pontt, and S. Kouro, "Multilevel voltage source converter topologies for industrial medium-voltage drives," IEEE Trans. Ind. Electron., vol. 54, no. 6, pp. 2930–2945, Dec. 2007.

[23] H. D. Bang, R. P. Roojj, A. S. McDonald, and M. A. Mueller, "10MWwind turbine direct drive generator design with pitch or active speed stall control," in Proc. IEEE IEMDC Conf., Antalya, Turkey, vol. 2, May 2007, pp. 1390–1395.

[24] X. Yuan, F. Wang, D. Boroyevich, Y. Li, and R. Burgos, "Dc-link voltage control of a full power converter for wind generator operating in weak-grid systems," IEEE Trans. Power Electron., vol. 24, no. 9, pp. 2178–2192, Sep. 2009.

[25] R. Cardenas and R. Pena, "Sensor less vector control of induction machines for variable-speed wind energy applications," IEEE Trans. Energy Convers., vol. 19, no. 1, pp. 196–205, Mar. 2004.

[26] P. J. Tavner, G. J. W. Bussel, and F. Spinato, "Machine and converter reliabilities in wind turbines," in Proc. IET PEMD'06 Conf., Dublin, Ireland, Mar. 2006, pp. 127–130.

[27] R. Teodorescu, F. Blaabjerg, M. Liserre, and P. C. Loh, "Proportional resonant controllers and filters for grid-connected voltage–source converters," IEE Proc. Elect. Power Appl., vol. 153, no. 5, pp. 750–762, Sep. 2006.

[28] R. Teodorescu, M. Liserre, and P. Rodriguez, Grid Converters for Photovoltaic and Wind Power Systems, Chap. 4. Hoboken, NJ, USA: Wiley, 2011.

[29] IGBT module datasheet [Online]. Available: http://www.infineon.com dgdl/

[30] S. Dieckerhoff, S. Bernet, and D. Krug Power, "Loss-oriented evaluation of high voltage IGBTs and multilevel converters in transformerless traction applications," IEEE Trans. Power Electron., vol. 20, no. 6, pp. 1328–1336, Nov. 2005.

ISSN No: 2348-4845
International Journal & Magazine of Engineering, Technology, Management and Research
A Peer Reviewed Open Access International Journal

Author Details

Miss. Sri **Nandini Balabommu** is pursuing M.Tech (Power Systems) at Kandula Srinivasa Reddy Memorial College of Engineering. She Completed her B.Tech(EEE) from Kottam College of Engineering, Kurnool, Andhra Pradesh, India.

Mr**. Bhaskar Reddy** member of IEI and IEEE member since 2002. He is acting as Secretary IEI Student Branch. Many IEI student branch activities are being run successfully under his esteemed Guidance. Areas of interest: Power systems, Electrical installation & Estimation(EIE), Power Electronics, Power Electronics and Drives, High Voltage DC Transmission and FACTS etc.